

Automated Clustering of High-dimensional Data with a Feature Weighted Mean Shift Algorithm*

Saptarshi Chakraborty^{†1}, Debolina Paul^{†2}, and Swagatam Das^{‡3}

¹Department of Statistics, University of California, Berkeley

²Indian Statistical Institute, Kolkata, India

³Electronics and Communication Sciences Unit, Indian Statistical Institute, Kolkata, India

Abstract

Mean shift is a simple interactive procedure that gradually shifts data points towards the mode which denotes the highest density of data points in the region. Mean shift algorithms have been effectively used for data denoising, mode seeking, and finding the number of clusters in a dataset in an automated fashion. However, the merits of mean shift quickly fade away as the data dimensions increase and only a handful of features contain useful information about the cluster structure of the data. We propose a simple yet elegant feature-weighted variant of mean shift to efficiently learn the feature importance and thus, extending the merits of mean shift to high-dimensional data. The resulting algorithm not only outperforms the conventional mean shift clustering procedure but also preserves its computational simplicity. In addition, the proposed method comes with rigorous theoretical convergence guarantees and a convergence rate of at least a cubic order. The efficacy of our proposal is thoroughly assessed through experimental comparison against baseline and state-of-the-art clustering methods on synthetic as well as real-world datasets.

1 Introduction

Clustering, a cornerstone of unsupervised learning, refers to the task of partitioning a dataset into more than one exhaustive and mutually exclusive groups, based on some measure of similarity (Xu and Tian, 2015). Some popular paradigms in clustering include center-based approaches such as k -means and its variants (Jain, 2010), hierarchical clustering (Carlsson and Mémoli, 2010), spectral clustering (Ng et al., 2002; Hess et al., 2019), density-based methods (Ester et al., 1996), convex clustering (Chi and Lange, 2015), kernel clustering (Dhillon et al., 2004), optimal transport based methods (Mi et al., 2018; Chakraborty et al., 2020a), model-based frequentist approaches (McNicholas, 2016) and Bayesian methods (Archambeau and Verleysen, 2007; Kulis and Jordan, 2012).

Most of the aforementioned algorithms inherently use the number of clusters (k) as an input. However, for real-world data, k may not be known beforehand. Determining k from the dataset itself has long been an open problem and has attracted a lot of attention from the relevant research community (Tibshirani et al., 2001; Hamerly and Elkan, 2004; Fischer, 2011; Kulis and Jordan, 2012; Chakraborty and Das, 2018; Gupta et al., 2018; Paul and Das, 2020).

Moreover, algorithms for solving k -means type non-convex clustering problems are prone to get stuck at local minima (Xu and Lange, 2019). Recent attempts to mitigate this issue approach the problem via annealing with a class of functions approximating the k -means type objective (Xu and Lange, 2019; Chakraborty et al., 2020b; Paul et al., 2020) or by taking a convex relaxation of the problem (Chi and Lange, 2015; Pelckmans et al., 2005; Wang et al., 2018). There are also density-based algorithms like DBSCAN (Ester et al., 1996; Jiang, 2017) or other mode seeking approaches like quick shift (Vedaldi and Soatto, 2008;

*To appear at the 35-th AAAI Conference on Artificial Intelligence, 2021.

[†]Joint first authors contributed equally to this work.

[‡]Correspondence to: swagatam.das@isical.ac.in

Jiang, 2017) which attempts to speed up mean shift. However, these methods either require k as an input or their performance degrade in a high-dimensional setting, where the signal-to-noise-ratio is quite low.

To find the number of clusters automatically and to learn various properties of the feature space, researchers have resorted to the mean shift (MS) paradigm (Cheng, 1995; Su and Shang, 2017). Mean shift has previously been used for mode seeking, object tracking, and automated clustering in the feature space.

Suppose $\mathcal{X} = \{\mathbf{x}_1, \dots, \mathbf{x}_n\} \subset \mathbb{R}^p$ be n data points to be clustered. The mean shift initiates n points $\mathbf{y}_1^{(0)}, \dots, \mathbf{y}_n^{(0)}$ and updates \mathbf{y}_i according to the following update rule:

$$\mathbf{y}_i^{(t+1)} = \frac{\sum_{j=1}^n K(\|\mathbf{y}_i^{(t)} - \mathbf{x}_j\|/h)\mathbf{x}_j}{\sum_{j=1}^n K(\|\mathbf{y}_i^{(t)} - \mathbf{x}_j\|/h)}, \quad (1)$$

until convergence. Here $K(\cdot)$ is a kernel function (e.g. the Gaussian kernel, $K(x) = \exp\{-x^2\}$) and h is the bandwidth parameter. This version of the mean shift is often used to detect the mode(s) of the estimated density. Often, instead of updating based on the original data points \mathbf{x}_i 's, one uses $\mathbf{y}_i^{(t)}$'s, the points obtained in the t -th step. In this case, the updates take the following form:

$$\mathbf{y}_i^{(t+1)} = \frac{\sum_{j=1}^n K(\|\mathbf{y}_i^{(t)} - \mathbf{y}_j^{(t)}\|/h)\mathbf{y}_j^{(t)}}{\sum_{j=1}^n K(\|\mathbf{y}_i^{(t)} - \mathbf{y}_j^{(t)}\|/h)}. \quad (2)$$

As before, $\mathbf{y}_i^{(0)}$ is initiated at \mathbf{x}_i . This version of mean shift is referred to as Blurring Mean Shift (BMS). The updates in equation (2) can be thought of as putting a low-pass filter on the data and thus "blurring" out irregularities in the data. Apart from clustering, BMS has been used for data denoising and manifold learning (Wang and Carreira-Perpinán, 2010).

Despite their simplicity, both the usual and blurring mean shift perform poorly for high-dimensional data. This is primarily because of the use of Euclidean distance, which becomes less informative as the number of feature increases due to the curse of dimensionality (Donoho et al., 2000). High-dimensional datasets often contain only a few relevant/ discriminating features, along with a huge number of irrelevant/noisy features, which severely affect the performance of mean shift and other popular clustering algorithms.

There is a rich literature on clustering high-dimensional data including subspace clustering (Kriegel et al., 2009; Elhamifar and Vidal, 2013), bi-clustering (Chi et al., 2017), dimensionality reduction based approaches (Jin et al., 2016) and data-depth based approaches (Sarkar and Ghosh, 2019). However, most of these methods are computationally expensive. Towards finding efficient feature representation of high-dimensional data while clustering, weighted k -means (Huang et al., 2005) and Sparse k -means (Witten and Tibshirani, 2010) have become benchmark algorithms for learning effective feature representations of such data. However, these methods also require k as input and thus, lose their appeal to the practitioner who may not have handled the data before and wants to find the number of clusters in an unsupervised manner as well.

This paper aims to develop a blurring mean shift based algorithm, which can automatically find an efficient feature representation of the data as well as the number of clusters *simultaneously*. Called the Weighted Blurring Mean Shift (WBMS), we extend the merits of blurring mean shift to high-dimensional data, while preserving its computational cost. To achieve this, we introduce a feature weight vector to learn the importance of each feature as the data is smoothed. The resulting iterations lead to an elegant and simple algorithm with closed-form updates. The weight update scheme follows the philosophy that features with higher within-cluster variance contribute less in finding the cluster structure of the data (Huang et al., 2005; Witten and Tibshirani, 2010; Chakraborty et al., 2020b). The main contributions of this paper can be summarized as follows:

- In Section 2, we introduce the Weighted Blurring Mean Shift (WBMS) formulation as an intuitive extension of mean shift to high-dimensional data clustering. This simple formulation is found to be effective in finding out the number of clusters and also filter out the unimportant features from the data *simultaneously*.
- As shown in Section 2.4, the obtained feature weights can be interpreted as the outcome of an entropy regularization on the within-cluster sum of squares.

- The WBMS algorithm comes with closed-form updates and its convergence guarantees are discussed in Section 3.1.
- We also analyze asymptotic convergence properties of the data cloud under the WBMS algorithm in Section 3.2. We analytically show that the convergence of the spread of the data cloud is at least of cubic order.
- Through detailed experimental analysis, we show the efficacy of our proposed algorithm against state-of-the-art clustering techniques on a suit of simulated and real-world data in Section 4. Our experimental results indicate that WBMS is especially effective, compared to its competitors, in a high-dimensional setting despite the low signal-to-noise-ratio.

Before proceeding to the details of WBMS, let us now present a motivating example demonstrating its potential.

1.0.1 A Motivating Example

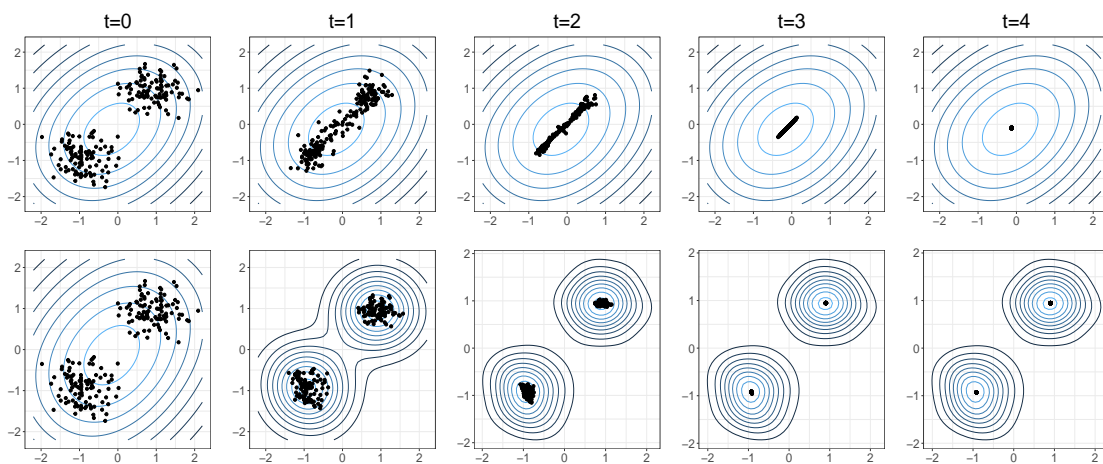


Figure 1: Performance of BMS (first row) and WBMS (second row) along with the contour plots of the estimated kernel density for the motivating example as the number of iterations (t) is increased. WBMS correctly identifies the two true cluster centroids and efficiently selects the relevant features, while the BMS fails to do so.

We generate a 200×32 dimensional data, called `data1`, which consists of two clusters with 100 points each. The cluster structure of `data1` is fully contained in the first two features and the rest of the 30 features are independently generated from a standard normal distribution, that contain no clustering information. We standardize (z -transform) the data before use and set the bandwidth $h = 0.1$. In Fig. 1, we show the position of the data cloud, plotted in the first two relevant feature dimensions, for both BMS and WBMS as the number of iterations (t) is increased. It can be easily seen that since BMS is more influenced by the combination of 30 Gaussian features, the data cloud gradually converges to the origin. On the other hand, the WBMS correctly identifies the two important and informative features. Thereby using this information, the data cloud converges to the two cluster centroids. The estimated density of the original data cloud \mathcal{X} , $\hat{f}(\mathbf{x}) \propto \sum_{i=1}^n \exp\{-\|\mathbf{x} - \mathbf{x}_i\|_{\mathbf{w}}^2/h\}$, with \mathbf{w} being the feature weights found out by WBMS (see Section 2 for the definition of $\|\cdot\|_{\mathbf{w}}$), also closely resembles the density of the data without the presence of the 30 non-informative features.

2 Weighted Blurring Means Shift

In this section, we formulate the Weighted Blurring Mean Shift (WBMS) algorithm and discuss some of its intriguing properties. Throughout this paper, $\mathcal{N}_p(\boldsymbol{\mu}, \Sigma)$ denotes the p -variate normal distribution with mean

μ and dispersion matrix Σ . $Unif(A)$ denotes the uniform distribution over the set A .

2.1 Motivation

Let $\mathbf{x}_1, \dots, \mathbf{x}_n \in \mathbb{R}^p$ be n data points to be clustered. We note that the blurring mean shift updates (equation (2)) uses the Euclidean distance $\|\mathbf{x} - \mathbf{y}\|_2 = \sqrt{\sum_{l=1}^p (x_l - y_l)^2}$. The Euclidean distance puts equal weight on each of the components $(x_l - y_l)^2$ and thus, not suitable when there are many noisy features, which are irrelevant to the clustering of the data. Recent research (Witten and Tibshirani, 2010; Chakraborty et al., 2020b) has been focused in replacing the usual Euclidean distance with the weighted distance $\|\mathbf{x} - \mathbf{y}\|_{\mathbf{w}} = \sqrt{\sum_{l=1}^p w_l (x_l - y_l)^2}$. Here $w_l \geq 0$ denotes the feature weight of the l -th feature. It can be easily checked that $\|\cdot\|_{\mathbf{w}}$ defines a norm on \mathbb{R}^p . A large feature weight, w_l on the l -th feature gives more importance to the difference $|x_l - y_l|$, the discrimination between \mathbf{x} and \mathbf{y} along the l -th coordinate vector. \mathbf{w} is called the feature weight vector and is usually normalized, i.e. $\mathbf{1}^\top \mathbf{w} = 1$. The feature weights are typically learned from the data and are updated every passing iteration. Normally, the feature weights are taken as some decreasing function of the within cluster sum of squares for that feature.

2.2 Formulation

We will use a similar update rule as in BMS (equation (2)). However, instead of the usual Euclidean distance, we will use the weighted distance $\|\cdot\|_{\mathbf{w}}$. The update rule for the data points is given by,

$$\mathbf{y}_i^{(t+1)} = \frac{\sum_{j=1}^n K(\|\mathbf{y}_i^{(t)} - \mathbf{y}_j^{(t)}\|_{\mathbf{w}^{(t)}}/h) \mathbf{y}_j^{(t)}}{\sum_{j=1}^n K(\|\mathbf{y}_i^{(t)} - \mathbf{y}_j^{(t)}\|_{\mathbf{w}^{(t)}}/h)}. \quad (3)$$

The feature weights are updated as follows:

$$w_l^{(t)} = \frac{\exp\{-\frac{1}{n\lambda} \sum_{i=1}^n (x_{il} - y_{il}^{(t)})^2\}}{\sum_{l'=1}^p \exp\{-\frac{1}{n\lambda} \sum_{i=1}^n (x_{il'} - y_{il'}^{(t)})^2\}}. \quad (4)$$

Algorithm 1 gives a formal description of the weighted blurring mean shift algorithm.

Algorithm 1 Weighted Blurring Mean Shift (WBMS) Algorithm

Input: $\mathbf{x}_1, \dots, \mathbf{x}_n \in \mathbb{R}^p$, $h, \lambda > 0$

Output: $\mathbf{y}_1, \dots, \mathbf{y}_n$ and \mathbf{w} .

Initialize $\mathbf{y}_i^{(0)} \leftarrow \mathbf{x}_i$ for all $i = 1, \dots, n$.

Initialize $w_l^{(0)} = \frac{1}{p}$, for all $l = 1, \dots, p$.

repeat

Step 1: Update \mathbf{y}_i 's by,

$$\mathbf{y}_i^{(t+1)} \leftarrow \frac{\sum_{j=1}^n K(\|\mathbf{y}_i^{(t)} - \mathbf{y}_j^{(t)}\|_{\mathbf{w}^{(t)}}/h) \mathbf{y}_j^{(t)}}{\sum_{j=1}^n K(\|\mathbf{y}_i^{(t)} - \mathbf{y}_j^{(t)}\|_{\mathbf{w}^{(t)}}/h)}.$$

Step 2: Update \mathbf{w} by,

$$w_l^{(t)} = \frac{\exp\{-\frac{1}{n\lambda} \sum_{i=1}^n (x_{il} - y_{il}^{(t)})^2\}}{\sum_{l'=1}^p \exp\{-\frac{1}{n\lambda} \sum_{i=1}^n (x_{il'} - y_{il'}^{(t)})^2\}}.$$

until $|\max_{i,j} \|\mathbf{y}_i^{(t+1)} - \mathbf{y}_j^{(t+1)}\|_2 - \max_{i,j} \|\mathbf{y}_i^{(t)} - \mathbf{y}_j^{(t)}\|_2|$ converges

2.3 Detecting the Clusters

We observe that Algorithm 1 outputs $\mathbf{y}_1, \dots, \mathbf{y}_n$, which are proxies for the cluster centroids. One should note that if \mathbf{x}_i and \mathbf{x}_j were originally in the same cluster, then \mathbf{y}_i and \mathbf{y}_j should be close to each other in

the Euclidean sense, i.e. $\|\mathbf{y}_i - \mathbf{y}_j\|_2$ should be small enough. We construct an undirected graph with the adjacency matrix $\mathbf{A} = ((a_{ij}))$. For a prefixed tolerance ϵ (in our experiments, we take $\epsilon = 10^{-5}$), we will take,

$$a_{ij} = \begin{cases} 1, & \text{if } \|\mathbf{y}_i - \mathbf{y}_j\|_2 < \epsilon \\ 0, & \text{Otherwise.} \end{cases}$$

Let \mathcal{G} be a graph based on the adjacency matrix \mathbf{A} and vertices $\mathbf{x}_1, \dots, \mathbf{x}_n$. The clusters in \mathcal{X} should ideally correspond to the connected components of \mathcal{G} . The number of clusters, k , corresponds to the number of connected components of \mathcal{G} . The connected components of \mathcal{G} can easily be found by a Depth First Search or a Breadth First Search.

2.4 Implicit Entropy Regularization

We now show that the weight update scheme presented in equation (4) can be thought of as the outcome of an entropy regularization. At convergence $\mathbf{y}_i^{(t)}$ can be treated as the cluster centroid corresponding to \mathbf{x}_i . Thus, the within cluster sum of squares is given by, $\frac{1}{n} \sum_{i=1}^n \|\mathbf{x}_i - \mathbf{y}_i^{(t)}\|_{\mathbf{w}}^2$. Since we are imposing the constraint $\sum_{l=1}^p w_l = 1$, minimization of this within cluster sum of squares will result in a trivial coordinate vector of \mathbb{R}^p . As observed by (Chakraborty et al., 2020b), this problem can be successfully avoided by adding an entropy incentive term as:

$$\frac{1}{n} \sum_{i=1}^n \|\mathbf{x}_i - \mathbf{y}_i^{(t)}\|_{\mathbf{w}}^2 + \lambda \sum_{l=1}^p w_l \log w_l, \quad (5)$$

where $\lambda > 0$. Note that the second term in the above expression is the negative of Shannon's entropy of \mathbf{w} . Minimizing (5) subject to $\mathbf{w}^\top \mathbf{1} = 1$, results in the weight update formula, given in equation (4). This is assured by the following theorem.

Theorem 1. *Let \mathbf{w}^* be the minimizer of (5), subject to $\mathbf{w}^\top \mathbf{1} = 1$. Then,*

$$w_l^* = \frac{\exp\{-\frac{1}{n\lambda} \sum_{i=1}^n (x_{il} - y_{il}^{(t)})^2\}}{\sum_{l'=1}^p \exp\{-\frac{1}{n\lambda} \sum_{i=1}^n (x_{il'} - y_{il'}^{(t)})^2\}}.$$

Proof. Problem (5) can be rewritten as follows:

$$\min_{\mathbf{w}} \sum_{l=1}^p D_l w_l + \lambda \sum_{l=1}^p w_l \log w_l$$

where $D_l = \frac{1}{n} \sum_{i=1}^n (x_{il} - y_{il}^{(t)})^2$.

This problem can now be solved using the constraints $\mathbf{w}^\top \mathbf{1} = 1$, $w_l \geq 0 \forall l = 1, \dots, p$. The Lagrangian is thus given by,

$$L = \sum_{l=1}^p D_l w_l + \lambda \sum_{l=1}^p w_l \log w_l - \alpha \left(\sum_{l=1}^p w_l - 1 \right)$$

Putting $\frac{\partial L}{\partial w_l} = 0$, we have,

$$D_l + \lambda(1 + \log w_l) - \alpha = 0$$

Thus, we have $w_l \propto \exp(-\frac{D_l}{\lambda})$.

Using the condition $\mathbf{w}^\top \mathbf{1} = 1$, we have,

$$\begin{aligned} w_l^* &= \frac{\exp(-\frac{D_l}{\lambda})}{\sum_{l'=1}^p \exp(-\frac{D_{l'}}{\lambda})} \\ &= \frac{\exp\{-\frac{1}{n\lambda} \sum_{i=1}^n (x_{il} - y_{il}^{(t)})^2\}}{\sum_{l'=1}^p \exp\{-\frac{1}{n\lambda} \sum_{i=1}^n (x_{il'} - y_{il'}^{(t)})^2\}}. \end{aligned}$$

This solution to the relaxed problem also satisfies the non-negativity condition. Hence the result. \square

3 Theoretical Properties and Convergence Guarantees

We will now discuss some of the interesting properties of WBMS. In particular, we prove that WBMS converges after a finite number of iterations for any fixed tolerance. We also find the asymptotic rate of convergence of the cluster variance as the number of points. Some related theoretical work in this area can be found in (Carreira-Perpiñán, 2006; Chen, 2015; Huang et al., 2018; Rocha et al., 2020).

3.1 Convergence Guarantee

In this section, we will discuss some of the theoretical properties of the WBMS algorithm. For any set $A \subseteq \mathbb{R}^p$, let $\mathcal{C}(A)$ denote the convex hull of A . We begin our analysis by proving that the convex hulls of $\{\mathbf{y}_1^{(t)}, \dots, \mathbf{y}_n^{(t)}\}$ for a decreasing sequence of sets in Theorem 2.

Theorem 2. *Let $C_t = \mathcal{C}(\{\mathbf{y}_1^{(t)}, \dots, \mathbf{y}_n^{(t)}\})$. Then $\{C_t\}_{t=0}^\infty$ constitutes a decreasing sequence of sets, i.e.*

$$C_0 \supseteq C_1 \supseteq \dots \supseteq C_t \supseteq C_{t+1} \supseteq \dots$$

Proof. From equation (3), we note that $\mathbf{y}_i^{(t+1)}$ can be represented as a convex combination of $\mathbf{y}_1^{(t)}, \dots, \mathbf{y}_n^{(t)}$. This implies that $\mathbf{y}_i^{(t+1)} \in C_t$, for all $i = 1, \dots, n$. Thus C_t is a convex set, which contains $\{\mathbf{y}_1^{(t+1)}, \dots, \mathbf{y}_n^{(t+1)}\}$. Since C_{t+1} is the smallest convex set containing $\{\mathbf{y}_1^{(t+1)}, \dots, \mathbf{y}_n^{(t+1)}\}$, $C_t \supseteq C_{t+1}$. \square

Since $\{C_t\}_{t=0}^\infty$ forms a decreasing sequence of sets, we immediately get that C_t converges in the following corollary.

Corollary 1. *$\lim_{t \rightarrow \infty} C_t$ exists and is given by, $\lim_{t \rightarrow \infty} C_t = \bigcap_{t=1}^\infty C_t$.*

Proof. $\{C_t\}_{t=1}^\infty$ constitutes a decreasing sequence of sets. The result directly follows from applying monotone convergence theorem for sets (Rudin, 1964). \square

In Theorem 3, we derive that for any fixed tolerance, the convergence criterion of Algorithm 1 is satisfied after a number of finite iterations.

Theorem 3. *For any pre-fixed tolerance level δ , there exists $T \in \mathbb{N}$ such that*

$$\left| \max_{i,j} \|y_i^{(t+1)} - y_j^{(t+1)}\|_2 - \max_{i,j} \|y_i^{(t)} - y_j^{(t)}\|_2 \right| < \delta,$$

for all $t \geq T$.

Proof. From Corollary 1, $\{C_t\}_{t=1}^\infty$. This implies that the vertices of C_t converges. Let $a_t = \max_{i,j} \|y_i^{(t)} - y_j^{(t)}\|_2$. Since a_t is a function of the vertices of C_t , $\{a_t\}_{t=1}^\infty$ also converges. Since $\{a_t\}_{t=1}^\infty$ is a convergent sequence of reals, $\{a_t\}_{t=1}^\infty$ is Cauchy (Rudin, 1964). Thus for any $\delta > 0$, there exists $T \in \mathbb{N}$ such that $\left| \max_{i,j} \|y_i^{(t+1)} - y_j^{(t+1)}\|_2 - \max_{i,j} \|y_i^{(t)} - y_j^{(t)}\|_2 \right| < \delta$, for all $t \geq T$. \square

3.2 Convergence Rate

Let us now discuss the behavior of a Gaussian cluster under WBMS. We will show that the Gaussian cluster shrinks towards its mean with at least a cubic convergence rate. Let $\phi(\mathbf{x}; \boldsymbol{\mu}, \boldsymbol{\Sigma})$ denote the Gaussian probability density function with mean $\boldsymbol{\mu}$ and dispersion matrix $\boldsymbol{\Sigma}$. In order to remove the dependency on the random process, we take an infinite sample, distributed in the whole of \mathbb{R}^p according to the density $q(\mathbf{x})$. For simplicity, we consider the Gaussian kernel. The kernel density estimate at \mathbf{z} , based on the data $\mathbf{y}_1^{(t)}, \dots, \mathbf{y}_n^{(t)}$ is given by,

$$\hat{p}_t(\mathbf{z}) = \frac{c(h, \mathbf{w}^{(t)})}{n} \sum_{j=1}^n \exp \left\{ - \|\mathbf{z} - \mathbf{y}_j^{(t)}\|_{\mathbf{w}^{(t)}}^2 / h \right\}.$$

Here $c(h, \mathbf{w}^{(t)})$ is a constant depending only on h and $\mathbf{w}^{(t)}$. From equation (3), we get,

$$\begin{aligned}
\mathbf{y}_i^{(t+1)} &= \frac{\sum_{j=1}^n \exp\{-\|\mathbf{y}_i^{(t)} - \mathbf{y}_j^{(t)}\|_{\mathbf{w}^{(t)}}^2/h\} \mathbf{y}_j^{(t)}}{\sum_{j=1}^n \exp\{-\|\mathbf{y}_i^{(t)} - \mathbf{y}_j^{(t)}\|_{\mathbf{w}^{(t)}}^2/h\}} \\
&= \frac{c(h, \mathbf{w}^{(t)})}{n} \sum_{j=1}^n \frac{\exp\{-\|\mathbf{y}_i^{(t)} - \mathbf{y}_j^{(t)}\|_{\mathbf{w}^{(t)}}^2/h\} \mathbf{y}_j^{(t)}}{\frac{c(h, \mathbf{w}^{(t)})}{n} \sum_{j=1}^n \exp\{-\|\mathbf{y}_i^{(t)} - \mathbf{y}_j^{(t)}\|_{\mathbf{w}^{(t)}}^2/h\}} \\
&= \frac{c(h, \mathbf{w}^{(t)})}{n} \sum_{j=1}^n \frac{\exp\{-\|\mathbf{y}_i^{(t)} - \mathbf{y}_j^{(t)}\|_{\mathbf{w}^{(t)}}^2/h\} \mathbf{y}_j^{(t)}}{\hat{p}_t(\mathbf{y}_i^{(t)})} \\
&\approx c(h, \mathbf{w}^{(t)}) \int \mathbf{y} \frac{\exp\{-\|\mathbf{y}_i^{(t)} - \mathbf{y}\|_{\mathbf{w}^{(t)}}^2/h\}}{p_t(\mathbf{y}_i^{(t)})} q_t(\mathbf{y}) d\mathbf{y} \\
&= \int \mathbf{y} \frac{\phi(\mathbf{y}_i^{(t)} - \mathbf{y}; 0, \frac{h}{2} \text{diag}(\frac{1}{\mathbf{w}^{(t)}}))}{p_t(\mathbf{y}_i^{(t)})} q_t(\mathbf{y}) d\mathbf{y}.
\end{aligned}$$

Thus, if the number of samples is large, each data point \mathbf{z} is replaced by the conditional expectation $E(\mathbf{y}|\mathbf{z}) = \int \mathbf{y} p_t(\mathbf{y}|\mathbf{z}) d\mathbf{y}$, where, $p_t(\mathbf{y}|\mathbf{z}) = \phi(\mathbf{z} - \mathbf{y}; 0, \frac{h}{2} \text{diag}(1/\mathbf{w}^{(t)})) q_t(\mathbf{y}) / p_t(\mathbf{z})$. For simplicity of exposition, we begin with \mathbf{x} , which follows a Gaussian distribution with mean $\mathbf{0}$ and dispersion matrix $\Sigma = \text{diag}(\sigma_1^2, \dots, \sigma_p^2)$. From the above analysis, it is clear that at a population level, the WBMS can be thought of as taking consecutive conditional expectations w.r.t $p_t(\mathbf{y}|\mathbf{x}_t)$. Here \mathbf{x}_t denote the population at the t -th step of the algorithm with $\mathbf{x}_0 = \mathbf{x}$. The following theorem asserts that \mathbf{x}_t is also normally distributed.

Theorem 4. *Let $\mathbf{x}_0 \sim \mathcal{N}_p(\mathbf{0}, \Sigma)$ and $\mathbf{x}_{t+1} = \int \mathbf{y} p_t(\mathbf{y}|\mathbf{x}_t) d\mathbf{y}$. Here $p_t(\cdot)$ denotes the distribution of \mathbf{x}_t and $p_t(\mathbf{y}|\mathbf{z}) = \phi(\mathbf{z} - \mathbf{y}; 0, \frac{h}{2} \text{diag}(1/\mathbf{w}^{(t)})) q_t(\mathbf{y}) / p_t(\mathbf{z})$. Then, $\mathbf{x}_t \sim \mathcal{N}_p(\mathbf{0}, \text{diag}((s_1^{(t)})^2, \dots, (s_p^{(t)})^2))$, with*

$$s_l^{(t+1)} = (1 + h(s_l^{(t)})^2 / 2w_l^{(t)})^{-1} s_l^{(t)}. \quad (6)$$

Proof. We first find the distribution of \mathbf{x}_t .

$$\begin{aligned}
p_1(\mathbf{y}|\mathbf{x}_0) &= \phi\left(\mathbf{x}_0 - \mathbf{y}; 0, \frac{h}{2} \text{diag}(1/\mathbf{w}^{(0)})\right) q_0(\mathbf{y}) / p_t(\mathbf{x}_0) \\
&\propto \phi\left(\mathbf{x}_0 - \mathbf{y}; 0, \frac{h}{2} \text{diag}(1/\mathbf{w}^{(0)})\right) q_0(\mathbf{y}) \\
&\propto \exp\left\{-\frac{1}{h} \sum_{l=1}^p w_l^{(0)} (y_l - x_l^{(0)})^2\right\} \exp\left\{-\sum_{l=1}^p y_l^2 / (2\sigma_l^2)\right\} \\
&\propto \exp\left\{-\frac{1}{2} \sum_{l=1}^p \frac{\left(y_l - \frac{2w_l^{(0)} x_l^{(0)} / h}{2w_l^{(0)} / h + 1 / \sigma_l^2}\right)^2}{\frac{1}{(2w_l^{(0)} / h + 1 / \sigma_l^2)}}\right\}.
\end{aligned}$$

Thus, $\mathbf{x}_1 = E(\mathbf{y}|\mathbf{x}_0) = \left(\frac{2w_1^{(0)} x_1^{(0)} / h}{2w_1^{(0)} / h + 1 / \sigma_1^2}, \dots, \frac{2w_p^{(0)} x_p^{(0)} / h}{2w_p^{(0)} / h + 1 / \sigma_p^2}\right)$. Thus \mathbf{x}_1 is also a Gaussian distribution, with mean $\mathbf{0}$ and dispersion matrix as $\text{Var}(\mathbf{x}_1) = \text{diag}((s_1^{(1)})^2, \dots, (s_p^{(1)})^2)$, with

$$s_l^{(1)} = \frac{2w_l^{(0)} s_0 / h}{2w_l^{(0)} / h + 1 / \sigma_l^2} = \frac{1}{1 + \frac{h}{2w_l^{(0)}} (s_l^{(0)})^2} s_l^{(0)}.$$

Here $s_l^{(0)} = \sigma_l$. By an inductive argument, it is easy to see that, \mathbf{x}_{t+1} is also a Gaussian distribution, with mean $\mathbf{0}$ and dispersion matrix as $\text{Var}(\mathbf{x}_{t+1}) = \text{diag}((s_1^{(t+1)})^2, \dots, (s_p^{(t+1)})^2)$, with $s_l^{(t+1)} = (1 + \frac{h}{2w_l^{(t)}} (s_l^{(t)})^2)^{-1} s_l^{(t)}$. \square

Thus, the sequence of standard deviations $\{s_l^{(t)}\}$ form a decreasing sequence, which is bounded below. Hence, by monotone convergence theorem of real sequences (Rudin, 1964), $\{s_l^{(t)}\}$ also converges. Let this limit be s_l . Hence $\{\mathbf{x}_l^t\}$, the l -th coordinate of \mathbf{x}_t , converges in distribution to either $\mathcal{N}(0, s_l^2)$ (if $s_l > 0$) or the degenerate distribution at 0 (if $s_l = 0$). We also observe that at a population level,

$$w_l^{(t)} = \frac{\exp\{-E(x_l^{(0)} - x_l^{(t)})^2/\lambda\}}{\sum_{l'=1}^p \exp\{-E(x_{l'}^{(0)} - x_{l'}^{(t)})^2/\lambda\}}.$$

Since $w_l^{(t)}$ is a continuous function of \mathbf{v}_t , where $\mathbf{v}_t = (E(x_1^{(0)} - x_1^{(t)})^2, \dots, E(x_p^{(0)} - x_p^{(t)})^2)$. Since \mathbf{x}_t converges in distribution, \mathbf{v}_t also converges, which in turn implies that $w_l^{(t)}$ converges. Let the limit be w . The following theorem asserts that $s_l^{(t)} \rightarrow 0$, as $t \rightarrow \infty$, which in turn implies that \mathbf{x}_t converges to $\mathbf{0}$, in distribution.

Theorem 5. *Let $\mathbf{x}_t, s_l^{(t)}$ be as in Theorem 4. Then, $s_l = \lim_{t \rightarrow \infty} s_l^{(t)} = 0$ and the order of convergence of $\{s_l^{(t)}\}_{t=1}^\infty$ is at least cubic. Moreover, the asymptotic rate of convergence of $\{s_l^{(t)}\}$ is $\frac{2w_l}{h}$.*

Proof. We first consider the case $\lim_{t \rightarrow \infty} w_l^{(t)} = 0$. From equation (6), we observe that $\lim_{t \rightarrow \infty} s_l^{(t+1)} = 0$. Now if $\lim_{t \rightarrow \infty} w_l^{(t)} > 0$, we take limit as $t \rightarrow \infty$ on both sides of equation (6) and get,

$$s_l = \frac{1}{1 + \frac{h}{2w_l}(s_l)^2} s_l \implies s_l = 0, \forall l = 1, \dots, p.$$

We will now find the order of convergence of s_l to zero. We say that the order of convergence is m if m is the largest integer such that

$$r_s = \lim_{t \rightarrow \infty} \frac{|s_l^{(t+1)} - s_l|}{|s_l^{(t)} - s_l|^m} = \lim_{t \rightarrow \infty} \frac{(s_l^{(t)})^{3-m}}{(s_l^{(t)})^2 + \frac{h}{2w_l}} < \infty.$$

This occurs at least for the case $m = 3$, i.e. the convergence rate of $\{s_l^{(t)}\}_{t=1}^\infty$ is at least cubic. If $m = 3$, the asymptotic rate of convergence is given by, $r_s = \frac{2w_l}{h}$. \square

Thus, the asymptotic convergence rate is smaller if w_l is smaller, meaning that if a feature is deemed to have smaller feature weight, i.e. little relevance in containing the cluster structure, the convergence along that feature is faster.

Also note that since \mathbf{x}_t converges in distribution to $\mathbf{0}$, $w_l^{(t)}$, being a bounded continuous function of \mathbf{x}_t also converge in distribution to

$$w_l = \frac{\exp\{-E(x_l^{(0)} - 0)^2/\lambda\}}{\sum_{l'=1}^p \exp\{-E(x_{l'}^{(0)} - 0)^2/\lambda\}} \propto \exp\{-\sigma_l^2/\lambda\}.$$

Thus, in limit, features with larger variances receive smaller feature weights compared to features with smaller variances.

4 Experimental Results

In this section, we compare WBMS with classical baselines and state-of-the-art automated clustering algorithms. To evaluate the performances, we use Normalized Mutual Information (NMI) (Vinh et al., 2010) and Adjusted Rand Index (ARI) (Hubert and Arabie, 1985) between the ground truth and the obtained partition. For both the indices, a value of 1 indicates perfect clustering while a value of 0 indicates completely random class labels. Since our algorithm is developed for automated clustering, apart from the baseline k -means (MacQueen, 1967), we compare our method with Blurring Mean Shift (BMS) (Wang and Carreira-Perpinán, 2010), Gaussian means (G -means) (Hamerly and Elkan, 2004), Dirichlet Process means (DP -means) (Kulis and Jordan, 2012), Entropy Weighted DP -means (EWDP) (Paul and Das, 2020), and the Robust Continuous Clustering (RCC) (Shah and Koltun, 2017) algorithm. For fair comparison against the other automated

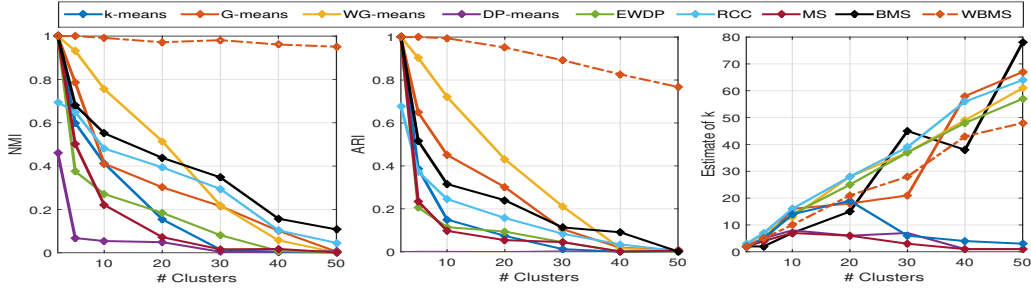


Figure 2: Performances of peer algorithms in terms of NMI (left), ARI (middle) and the estimated number of clusters (right) as the number of clusters increases in simulation 1. It is easily observed that WBMS consistently resembles the ground truth, while the other algorithms fail.

clustering methods, the number of clusters in k -means is supplied through the Gap statistics method (Tibshirani et al., 2001). It should be noted WG -means and RCC already entails higher computational complexity and we do not consider other alternative clustering techniques, which require k as an input. Since k -means and G -means depend on the random seeding, we run each algorithm 20 times independently on each data and the report the average performance. All the datasets are normalized (z -transform) before use. In our experiments, we use the Gaussian kernel. We observed that for the proposed algorithm, $h \in (0.1, 1)$ and $\lambda \in [1, 20]$ preserves a consistently good level of performance. All the other algorithms are tuned using their standard protocols. A pertinent ablation study is provided in the Appendix. Additional experiments and runtime comparisons also appear therein. For the sake of reproducibility, all the codes and datasets are available at <https://github.com/SaptarshiC98/WBMS>.

4.1 Simulation Studies

We now discuss the behavior of the peer algorithms through a set of simulation studies.

4.1.1 Simulation 1: Effect of increasing k

We now examine the behavior of the WBMS algorithm as the number of cluster k increases. In this simulation study, we take $n = 20 \times k$, $p = 20$, while k varies from 2 to 50. Let Θ be the $k \times p$ real matrix, whose rows represent the k cluster centroids. We generate Θ as follows.

- Generate $\theta_{jl} \sim Unif(0, 1)$ independently for $j = 1, \dots, k$ and $l = 1, \dots, 5$.
- Set $\theta_{jl} = 0$ for $j = 1, \dots, k$ and $l = 6, \dots, 20$.

After generating Θ , we generate the $n \times p$ data matrix \mathbf{X} as:

$$c_i \sim Unif(\{1, \dots, k\}); x_{il} \sim \mathcal{N}_1(\theta_{c_i, l}, 0.02^2) \text{ if } l \in \{1, \dots, 5\}$$

$$x_{il} \sim \mathcal{N}_1(0, 1) \text{ if } l \in \{6, \dots, 20\}.$$

From the data generation procedure, it is easy to observe that only the first five features contain the cluster structure of the data. We run all the peer algorithms on each of the datasets. Fig. 2 shows the average NMI and ARI values between the ground truth and the obtained partition. We also plot the average estimated number of clusters (\hat{k}) against the true number of clusters (k). It can be easily observed that WBMS consistently outperforms the other peer algorithms not only in terms of clustering performance but also in finding the true number of clusters.

4.1.2 Simulation 2: Effect of increasing p

This experiment assesses the performance of WBMS as the number of features grows. We generate $n = 100$ observations with $k = 4$ clusters. We increase the dimension from $p = 20$ to $p = 200$ at the difference of 20

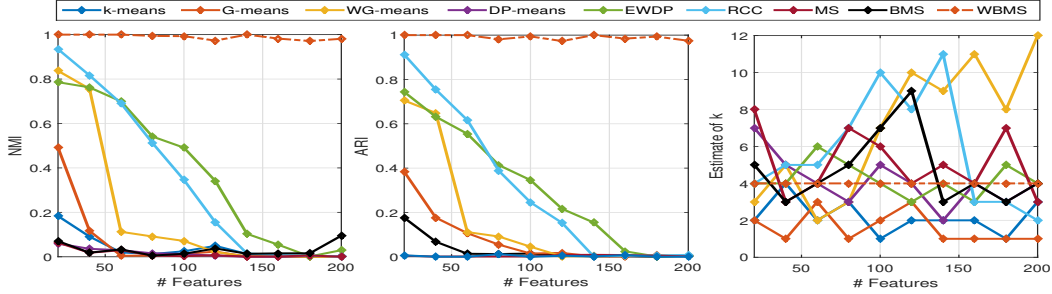


Figure 3: Performances of peer algorithms in terms of NMI (left), ARI (middle) and the estimated number of clusters (right) as the number of features increases in simulation 2. It is easily observed that WBMS consistently resembles the ground truth, while the other algorithms fail as the dimensionality of the data increases.

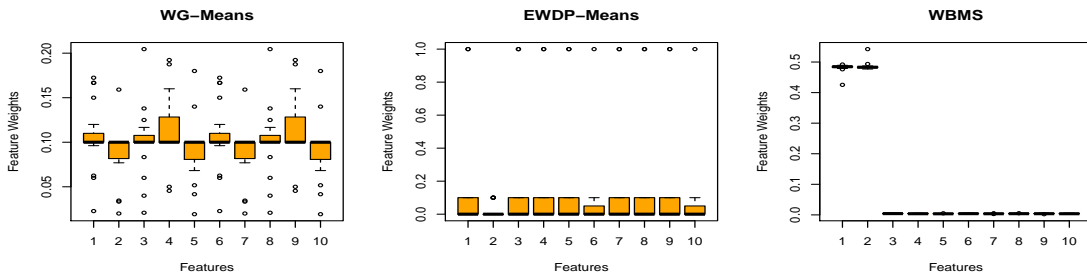


Figure 4: Boxplot shows that WBMS consistently identifies true features while WG-means and EWDP-means fail to do so.

to observe the effect of growing features. In each case, the number of informative features is fixed at 5% of the total number of features with an exception for the case $p = 20$, where we take 2 informative features. The clusters are spherical without any overlaps and are generated from Normal distributions with variance 0.3 and means generated from $Unif(0, 1)$ distribution. The non-informative features are generated from $\mathcal{N}_1(0, 1)$. Fig. 3 compares the NMI, ARI and estimated number of clusters for all the peer algorithms. From Fig. 3, we can easily observe that among all peer algorithms, not only the WBMS algorithm performs best in terms of NMI and ARI values, it also estimates the number of clusters perfectly.

4.1.3 Simulation 3: Feature Selection

We now examine the feature weighting properties of WBMS. Here, we take $n = 100$, $p = 10$, $k = 4$ and follow the data generation procedure described in Simulation 2. Without loss of generality, we take the first two features to be informative that actually contain the cluster structure. We compare the feature weights obtained by WBMS against those obtained by WG -means and EWDP. We record the feature weights obtained by these two algorithms along with proposed WBMS over 100 replicates of the data. The box plots for these 100 optimal feature weights are shown in Fig. 4 for all the three algorithms. The proposed WBMS successfully assigns almost all weights to informative features 1 and 2, even in this low signal-to-noise-ratio situation. Meanwhile, its peers WG -means and EWDP fail to do so.

4.2 Case Study on Glioma Data

We now evaluate the performance of our algorithm with a specific case study on the microarray dataset, Glioma (Nutt et al., 2003). The dataset comprises of 4434 gene expression levels, collected over 50 samples. There are four natural classes in the data viz. Glioblastomas (CG), Non-cancer Glioblastomas (NG), Cancer Oligodendrogliomas (CO), and Non-cancer Oligodendrogliomas (NO). In our experimental study, we compare

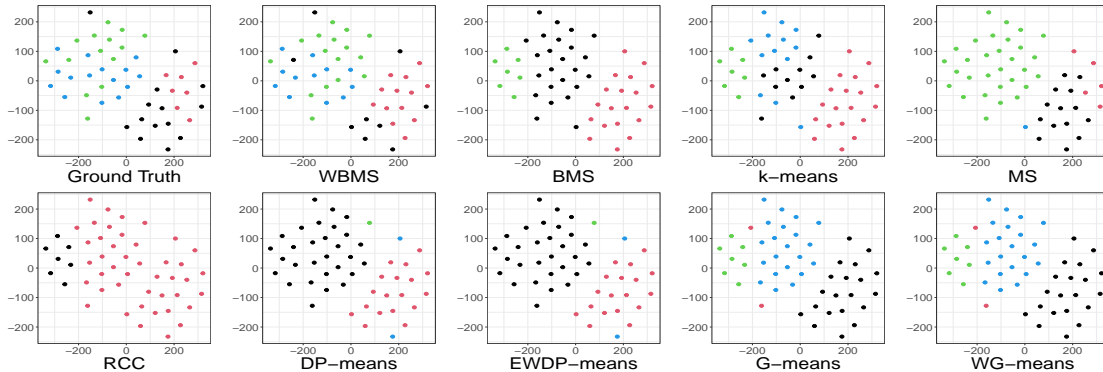


Figure 5: t -SNE plots for the GLIOMA dataset, color-coded by the partitions obtained by each peer algorithm.

our proposed WBMS algorithm to all the algorithms described in Section 4.1. To visualize the clustering results, we perform a t -SNE (Maaten and Hinton, 2008) and show the resulting embedding in Fig. 5, color-coded with the partitions obtained from the peer algorithms. WBMS closely represents the ground truth compared to its competitors. This is also easily seen from Table 2.

4.3 Performance on Real Data Benchmarks

Datasets	# Datapoints	# Features	# Clusters
GLIOMA	50	4434	4
Appendicitis	107	7	2
Zoo	101	16	7
Mammographic	830	5	2
Yale	165	1024	15
nci9	60	9712	9
Lymphoma	62	4026	3
Movement Libras	360	90	15
GCM	191	16063	15

Table 1: The dimensions of various real data, used in our experiments along with the true number of clusters.

To further demonstrate the efficacy of our proposal, we compare WBMS with the peer algorithms on eight benchmark real datasets. The datasets are taken from the UCI machine learning repository¹ (Dua and Graff, 2017), Keel repository² (Alcalá-Fdez et al., 2011) and ASU feature selection repository³ (Li et al., 2018). The microarray GCM data is collected from (Ramaswamy et al., 2001). The data dimensions are reported in Table 1. We follow the same computational protocols as stated at the beginning of Section 4. The performance of each algorithm, in terms of NMI and ARI, is reported in Table 2, which clearly indicate the superior performance of WBMS on each of the nine real data benchmarks.

5 Discussions

Despite decades of advancement, there is no proper solution for finding the number of clusters and feature weights simultaneously in the clustering problem. For high dimensional datasets, which contain a significant number of non-informative features, most of the existing automated clustering methods fail to identify the

¹<https://archive.ics.uci.edu/ml/index.php>

²<https://sci2s.ugr.es/keel/datasets.php>

³<http://featureselection.asu.edu/>

Datasets	Method	k -Means	G-Means	WG-Means	DP-Means	EWDP	RCC	MS	BMS	WBMS
GLIOMA	NMI	0.499	0.522	0.517	0.576	0.675	0.113	0.580	0.546	0.706
	ARI	0.328	0.367	0.373	0.416	0.598	0.004	0.429	0.398	0.618
Appendicitis	NMI	0.157	0.165	0.185	0.158	0.189	0.193	0.008	0.195	0.249
	ARI	0.230	0.169	0.188	0.231	0.188	0.000	0.014	0.223	0.434
Zoo	NMI	0.741	0.801	0.749	0.611	0.859	0.557	0.706	0.841	0.925
	ARI	0.459	0.646	0.559	0.452	0.872	0.039	0.436	0.867	0.953
Mammographic	NMI	0.231	0.181	0.240	0.191	0.273	0.181	0.181	0.008	0.348
	ARI	0.292	0.209	0.293	0.257	0.247	0.001	0.150	0.001	0.351
Yale	NMI	0.539	0.417	0.521	0.324	0.334	0.268	0.548	0.222	0.693
	ARI	0.271	0.173	0.227	0.040	0.061	0.031	0.069	0.027	0.485
nci9	NMI	0.458	0.394	0.394	0.181	0.211	0.143	0.346	0.394	0.686
	ARI	0.187	0.100	0.100	0.005	0.018	0.005	0.011	0.086	0.419
Lymphoma	NMI	0.441	0.592	0.690	0.518	0.648	0.243	0.241	0.595	0.778
	ARI	0.269	0.340	0.463	0.088	0.431	0.001	0.000	0.458	0.604
Movement	NMI	0.591	0.231	0.328	0.333	0.465	0.639	0.245	0.503	0.663
Libras	ARI	0.309	0.068	0.123	0.113	0.217	0.014	0.090	0.185	0.532
GCM	NMI	0.532	0.484	0.497	0.025	0.497	0.637	0.456	0.649	0.833
	ARI	0.288	0.248	0.266	0.002	0.266	0.361	0.413	0.536	0.714

Table 2: Performance Analysis on Real Life Datasets in terms of NMI & ARI values.

discriminating features as well as the number of clusters, resulting in poor performance. To circumvent such difficulties, in this paper, we put forth a novel clustering algorithm known as the Weighted Blurring Mean Shift (WBMS), which not only provides an efficient feature representation of the data but also detects the number of clusters simultaneously. WBMS comes with closed-form updates and rigorous convergence guarantees. We have also mathematically proved that under the nominal assumption of normality of the clusters, WBMS has at least a cubic convergence rate. Through detailed experimental analysis on simulated and real data, WBMS is particularly shown to be useful for high-dimensional data with many clusters.

References

- Alcalá-Fdez, J., Fernández, A., Luengo, J., Derrac, J., García, S., Sánchez, L., and Herrera, F. (2011). Keel data-mining software tool: data set repository, integration of algorithms and experimental analysis framework. *Journal of Multiple-Valued Logic & Soft Computing*, 17.
- Archambeau, C. and Verleysen, M. (2007). Robust bayesian clustering. *Neural Networks*, 20(1):129–138.
- Carlsson, G. and Mémoli, F. (2010). Characterization, stability and convergence of hierarchical clustering methods. *J. Mach. Learn. Res.*, 11:1425–1470.
- Carreira-Perpiñán, M. Á. (2006). Fast nonparametric clustering with gaussian blurring mean-shift. In *Proceedings of the 23rd international conference on Machine learning*, pages 153–160.
- Chakraborty, S. and Das, S. (2018). Simultaneous variable weighting and determining the number of clusters—a weighted gaussian means algorithm. *Statistics & Probability Letters*, 137:148–156.
- Chakraborty, S., Paul, D., and Das, S. (2020a). Hierarchical clustering with optimal transport. *Statistics & Probability Letters*, page 108781.
- Chakraborty, S., Paul, D., Das, S., and Xu, J. (2020b). Entropy weighted power k-means clustering. In *International Conference on Artificial Intelligence and Statistics*, pages 691–701. PMLR.
- Chen, T.-L. (2015). On the convergence and consistency of the blurring mean-shift process. *Annals of the Institute of Statistical Mathematics*, 67(1):157–176.
- Cheng, Y. (1995). Mean shift, mode seeking, and clustering. *IEEE transactions on pattern analysis and machine intelligence*, 17(8):790–799.

- Chi, E. C., Allen, G. I., and Baraniuk, R. G. (2017). Convex biclustering. *Biometrics*, 73(1):10–19.
- Chi, E. C. and Lange, K. (2015). Splitting methods for convex clustering. *Journal of Computational and Graphical Statistics*, 24(4):994–1013.
- Dhillon, I. S., Guan, Y., and Kulis, B. (2004). Kernel k-means: spectral clustering and normalized cuts. In *Proceedings of the tenth ACM SIGKDD international conference on Knowledge discovery and data mining*, pages 551–556.
- Donoho, D. L. et al. (2000). High-dimensional data analysis: The curses and blessings of dimensionality. *AMS math challenges lecture*, 1(2000):32.
- Dua, D. and Graff, C. (2017). UCI machine learning repository.
- Elhamifar, E. and Vidal, R. (2013). Sparse subspace clustering: Algorithm, theory, and applications. *IEEE Transactions on Pattern Analysis and Machine Intelligence*, 35(11):2765–2781.
- Ester, M., Kriegel, H.-P., Sander, J., Xu, X., et al. (1996). A density-based algorithm for discovering clusters in large spatial databases with noise. In *Kdd*, volume 96, pages 226–231.
- Fischer, A. (2011). On the number of groups in clustering. *Statistics & Probability Letters*, 81(12):1771–1781.
- Gupta, A., Datta, S., and Das, S. (2018). Fast automatic estimation of the number of clusters from the minimum inter-center distance for k-means clustering. *Pattern Recognition Letters*, 116:72 – 79.
- Hamerly, G. and Elkan, C. (2004). Learning the k in k-means. In *Advances in neural information processing systems*, pages 281–288.
- Hess, S., Duivesteyn, W., Honysz, P., and Morik, K. (2019). The spectacl of nonconvex clustering: a spectral approach to density-based clustering. In *Proceedings of the AAAI Conference on Artificial Intelligence*, volume 33, pages 3788–3795.
- Huang, J. Z., Ng, M. K., Rong, H., and Li, Z. (2005). Automated variable weighting in k-means type clustering. *IEEE Transactions on Pattern Analysis and Machine Intelligence*, 27(5):657–668.
- Huang, K., Fu, X., and Sidiropoulos, N. D. (2018). On convergence of epanechnikov mean shift. In *AAAI*.
- Hubert, L. and Arabie, P. (1985). Comparing partitions. *Journal of classification*, 2(1):193–218.
- Jain, A. K. (2010). Data clustering: 50 years beyond k-means. *Pattern Recognition Letters*, 31(8):651 – 666. Award winning papers from the 19th International Conference on Pattern Recognition (ICPR).
- Jiang, H. (2017). Density level set estimation on manifolds with dbscan. *arXiv preprint arXiv:1703.03503*.
- Jin, J., Wang, W., et al. (2016). Influential features pca for high dimensional clustering. *The Annals of Statistics*, 44(6):2323–2359.
- Kriegel, H.-P., Kröger, P., and Zimek, A. (2009). Clustering high-dimensional data: A survey on subspace clustering, pattern-based clustering, and correlation clustering. *ACM Transactions on Knowledge Discovery from Data (TKDD)*, 3(1):1–58.
- Kulis, B. and Jordan, M. I. (2012). Revisiting k-means: New algorithms via Bayesian nonparametrics. In *Proceedings of the 29th International Conference on Machine Learning, ICML 2012, Edinburgh, Scotland, UK, June 26 - July 1, 2012*.
- Li, J., Cheng, K., Wang, S., Morstatter, F., Trevino, R. P., Tang, J., and Liu, H. (2018). Feature selection: A data perspective. *ACM Computing Surveys (CSUR)*, 50(6):94.
- Maaten, L. v. d. and Hinton, G. (2008). Visualizing data using t-sne. *Journal of machine learning research*, 9(Nov):2579–2605.

- MacQueen, J. (1967). Some methods for classification and analysis of multivariate observations. In *Proceedings of the fifth Berkeley symposium on mathematical statistics and probability*, volume 1, pages 281–297. Oakland, CA, USA.
- McNicholas, P. D. (2016). Model-based clustering. *Journal of Classification*, 33(3):331–373.
- Mi, L., Zhang, W., Gu, X., and Wang, Y. (2018). Variational wasserstein clustering. In *Proceedings of the European Conference on Computer Vision (ECCV)*, pages 322–337.
- Ng, A. Y., Jordan, M. I., and Weiss, Y. (2002). On spectral clustering: Analysis and an algorithm. In *Advances in Neural Information Processing Systems*, pages 849–856.
- Nutt, C. L., Mani, D., Betensky, R. A., Tamayo, P., Cairncross, J. G., Ladd, C., Pohl, U., Hartmann, C., McLaughlin, M. E., Batchelor, T. T., et al. (2003). Gene expression-based classification of malignant gliomas correlates better with survival than histological classification. *Cancer research*, 63(7):1602–1607.
- Paul, D., Chakraborty, S., Das, S., and Xu, J. (2020). Kernel k-means, by all means: Algorithms and strong consistency. *arXiv preprint arXiv:2011.06461*.
- Paul, D. and Das, S. (2020). A bayesian non-parametric approach for automatic clustering with feature weighting. *Stat*, page e306.
- Pelckmans, K., De Brabanter, J., Suykens, J. A., and De Moor, B. (2005). Convex clustering shrinkage. In *PASCAL Workshop on Statistics and Optimization of Clustering Workshop*.
- Ramaswamy, S., Tamayo, P., Rifkin, R., Mukherjee, S., Yeang, C.-H., Angelo, M., Ladd, C., Reich, M., Latulippe, E., Mesirov, J. P., et al. (2001). Multiclass cancer diagnosis using tumor gene expression signatures. *Proceedings of the National Academy of Sciences*, 98(26):15149–15154.
- Rocha, P., Pinheiro, D., Cadeiras, M., and Bastos-Filho, C. (2020). Towards automatic clustering analysis using traces of information gain: The infoguide method. *arXiv preprint arXiv:2001.08677*.
- Rudin, W. (1964). *Principles of mathematical analysis*, volume 3. McGraw-hill New York.
- Sarkar, S. and Ghosh, A. K. (2019). On perfect clustering of high dimension, low sample size data. *IEEE Transactions on Pattern Analysis and Machine Intelligence*.
- Shah, S. A. and Koltun, V. (2017). Robust continuous clustering. *Proceedings of the National Academy of Sciences*, 114(37):9814–9819.
- Su, M. and Shang, Y. (2017). Solving fixed-point problems with inequality and equality constraints via a non-interior point homotopy path-following method. *Mathematical Problems in Engineering*, 2017.
- Tibshirani, R., Walther, G., and Hastie, T. (2001). Estimating the number of clusters in a data set via the gap statistic. *Journal of the Royal Statistical Society: Series B (Statistical Methodology)*, 63(2):411–423.
- Vedaldi, A. and Soatto, S. (2008). Quick shift and kernel methods for mode seeking. In *European conference on computer vision*, pages 705–718. Springer.
- Vinh, N. X., Epps, J., and Bailey, J. (2010). Information theoretic measures for clusterings comparison: Variants, properties, normalization and correction for chance. *The Journal of Machine Learning Research*, 11:2837–2854.
- Wang, B., Zhang, Y., Sun, W. W., and Fang, Y. (2018). Sparse convex clustering. *Journal of Computational and Graphical Statistics*, 27(2):393–403.
- Wang, W. and Carreira-Perpinán, M. A. (2010). Manifold blurring mean shift algorithms for manifold denoising. In *2010 IEEE Computer Society Conference on Computer Vision and Pattern Recognition*, pages 1759–1766.

Witten, D. M. and Tibshirani, R. (2010). A framework for feature selection in clustering. *Journal of the American Statistical Association*, 105(490):713–726.

Xu, D. and Tian, Y. (2015). A comprehensive survey of clustering algorithms. *Annals of Data Science*, 2(2):165–193.

Xu, J. and Lange, K. (2019). Power k-means clustering. In *International Conference on Machine Learning*, pages 6921–6931.

A Optimal Parameter values for Real-Life Datasets

In this section, we provide the optimal parameter values for real-life datasets. The experimental results for WBMS that are provided in Table 2 are based on the optimal parameter values provided in Table 3.

Datasets	h	λ
GLIOMA	0.5	1
Appendicitis	1	10
Zoo	0.8	20
Mammographic	0.8	10
Yale	0.1	10
nci9	0.1	5
Lymphoma	0.5	5
Movement Libras	0.1	10

Table 3: Optimal Parameter Values for Real-Life Datasets

B Ablation Studies

B.1 Abalation Study on h

In this section, we conduct an ablation study to assess the performance of the proposed WBMS algorithm for different values of h . We take $h = 0.1, 0.5, 0.8$ and 1 for our experimental study. The algorithm is run according to the procedure described in Section 4. As a cluster validity index, we use the ARI values between the ground truth and the obtained partition. We choose λ corresponding to the highest ARI value. Table 4 gives the ARI values for all the real-life datasets used in our experiments for different values of h .

Datasets	$h = 0.1$	$h = 0.5$	$h = 0.8$	$h = 1$
GLIOMA	0.587	0.618	0.618	0.524
Appendicitis	0.218	0.324	0.401	0.434
Zoo	0.953	0.912	0.754	0.754
Mammographic	0.212	0.295	0.351	0.320
Yale	0.485	0.414	0.234	0.001
nci9	0.419	0.419	0.340	0.108
Lymphoma	0.589	0.604	0.544	0.330
Movement Libras	0.532	0.414	0.021	0.001
GCM	0.714	0.531	0.531	0.562

Table 4: Average ARI values for WBMS on real-datasets for different values of h

Datasets	$\lambda = 1$	$\lambda = 5$	$\lambda = 10$	$\lambda = 20$
GLIOMA	0.618	0.618	0.618	0.510
Appendicitis	0.257	0.352	0.434	0.398
Zoo	0.717	0.717	0.906	0.953
Mammographic	0.198	0.202	0.351	0.351
Yale	0.055	0.414	0.485	0.423
nci9	0.210	0.419	0.419	0.378
Lymphoma	0.167	0.604	0.503	0.503
Movement Libras	0.251	0.376	0.532	0.532
GCM	0.510	0.714	0.714	0.714

Table 5: Average ARI values for WBMS on real-datasets for different values of λ

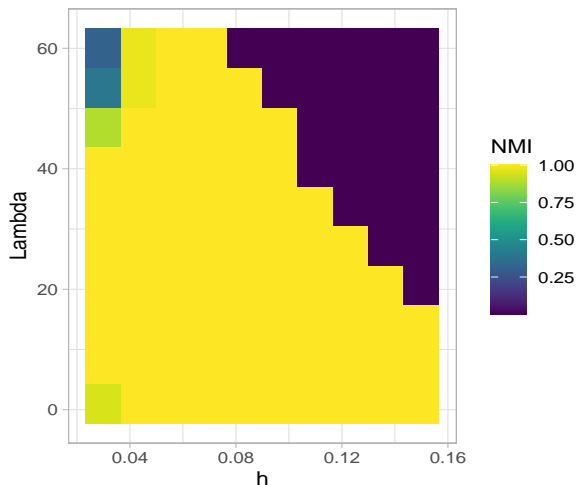


Figure 6: Heatmap of NMI values, plotted against different values of h and λ , showing that the WBMS is able to recover the perfect clustering (colored in yellow) over a considerable range of the hyper-parameter values.

B.2 Abalation Study on λ

For each of the optimal h , described in the previous section, we assess the performance of WBMS for different values of λ . Since, $\lambda \in [1, 20]$, we take $\lambda = 1, 5, 10$ and 20 . For each different value of λ , we run the algorithm similar to the procedure described in Section 4. We choose h corresponding to the highest ARI value. For ties, any value of h between the ties can be taken as optimal. Table 5 summarizes the ARI values for all real-life datasets used in our experiments for different values of λ .

B.3 Sensitivity Analysis

We also conducted a sensitivity analysis on a toy example with two clusters, each containing 100 points. The first two features of the dataset fully contains the cluster structure of the data, while the rest 30 are simulated independently from a standard normal distribution. For different values of h and λ , we run the WBMS and compute the NMI values between the ground truth and the obtained partition. In Fig. 6, we show the heatmap of NMI values, plotted against different values of h and λ . The hetmap clearly shows that the WBMS is able to recover the perfect clustering (colored in yellow) over a considerable range of the hyper-parameter values.

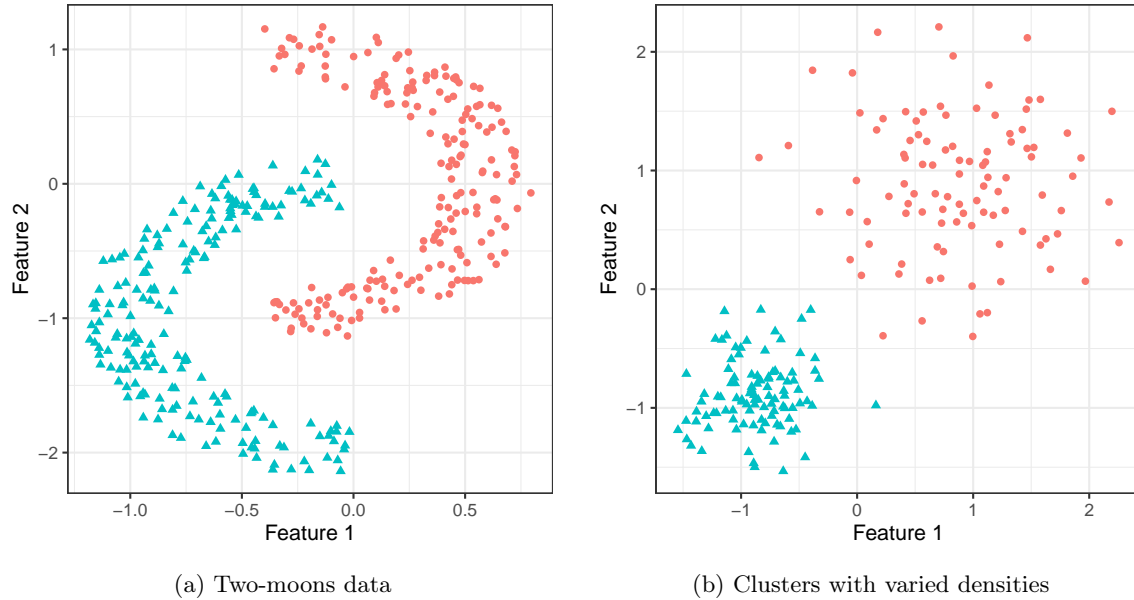


Figure 7: Performance of WBMS on some classic synthetic data.

C Additional Experiments

In this section we show the performance of WBMS on some standard datasets, where mean shift performs perfect clustering, whereas classical centroid-based algorithms fail to do so. To make the problems harder, we appended an additional 30 features, simulated from a standard normal distribution to the data matrix. In Fig. 7, it is easily observed that WBMS performs a perfect clustering on these datasets.